

Sedimenting Elastic Filaments in Turbulent Flows

Rahul K. Singh,^{1,*} Jason R. Picardo,² and Samridhi Sankar Ray¹

¹*International Centre for Theoretical Sciences, Tata Institute of Fundamental Research, Bangalore 560089, India*

²*Department of Chemical Engineering, Indian Institute of Technology Bombay, Mumbai 400076, India*

We investigate the gravitational settling of a long, model elastic filament in homogeneous isotropic turbulence. We show that the flow produces a strongly fluctuating settling velocity, whose mean is moderately enhanced over the still-fluid terminal velocity, and whose variance has a power-law dependence on the filament's weight but is surprisingly unaffected by its elasticity. In contrast, the tumbling of the filament is shown to be closely coupled to its stretching, and manifests as a Poisson process with a tumbling time that increases with the elastic relaxation time of the filament.

Sediments in turbulent flows are commonplace in nature and industry. Even so, theoretical progress in understanding how objects settle under gravity while being buffeted by a turbulent carrier flow is recent. Even in the simplest case of tiny rigid spherical particles, the interaction of these forces is rather intricate and leads to an enhancement of the settling velocity over its value in a still fluid—a fact that has been theoretically understood and quantified over just the past decade or so [1–7]. More recent work has addressed the issue of how spheroidal particles, with additional rotational degrees of freedom, orient themselves while settling [8, 9]. A common feature of these prior studies is that they are limited to rigid particles whose sizes, regardless of their anisotropy, are much smaller than the dissipative Kolmogorov scale η of the flow. These constraints are certainly meaningful for a wide variety of applications, such as understanding the initiation of rain in warm clouds [10–14] and the radiative properties of cold clouds [15–18], which involve, respectively, turbulent suspensions of spherical water droplets and non-spherical ice crystals.

However, sediments that are both deformable and larger than the Kolmogorov scale are just as ubiquitous. One important example is the sedimentation of long deformable filaments, wherein flow-induced deformation modifies the net drag force experienced by the filament [19], thus coupling the dynamics of conformation to settling. This problem has been recently addressed for low Reynolds number, non-turbulent flows [20]. However, understanding the gravitational settling of filaments when the carrier flow is turbulent (as encountered in papermaking [21] and the fields of marine ecology and pollution [22–25]) remains an important open problem.

In this paper, we address this issue through a combination of scaling analysis and detailed numerical simulations on a model elastic filament in a homogeneous and isotropic turbulent flow. In particular, we show that the turbulent flow produces strong fluctuations in the settling velocity, while moderately enhancing its mean value over the terminal value in a still-fluid. We theoretically derive how the normalised variance of the settling velocity scales with the elasticity and inertia (mass) of the filament, as well as with the relative strengths of the

accelerations due to gravity and turbulence. Our estimates are then verified through detailed numerical simulations. Furthermore, borrowing ideas from the persistence problem of non-equilibrium statistical physics, we uncover a close connection between the two internal motions of tumbling and stretching, which accompany the unsteady yet inevitable descent of the filament.

A simple model of a long filament, which retains enough internal structure to exhibit both elasticity and inertia, is a chain of heavy inertial particles connected through elastic springs [26]. Such chains are a useful framework to understand the intricate interplay between elasticity and turbulent mixing [27–29] and provide insights which complement those obtained from other models of fibres [30–33]. In this context, the most striking feature of filaments such as those we study is the manner in which they preferentially sample the geometry of a turbulent flow: in the inertia-less (neutrally buoyant) limit, such chains preferentially sample the vortical regions of the flow, in both two and three dimensions (3D) though for different reasons [27, 29]. This prediction, for the case of rigid chains in 3D, was recently confirmed experimentally [34]. The introduction of inertia (without gravity), counter-acts this tendency due to centrifugal expulsion from vortices and decorrelation from the flow, resulting in rather distinct dynamics [28]. Here, we account for gravitational acceleration and investigate the settling dynamics of these *elasto-inertial* chains.

We model a filament of mass M as a chain of N_b spherical beads. Considering ρ to be the mass density of the filament, we distribute the mass uniformly over the beads, each of radius $a \ll \eta$, so that $\frac{4}{3}\pi a^3 \rho N_b = M$. The beads are then characterised by a Stokesian relaxation time $\tau_p = \frac{2\rho a^2}{9\rho_f \nu}$, where ρ_f and ν are the density and kinematic viscosity of the carrier fluid. Each bead, positioned instantaneously at \mathbf{x}_j , is connected to its nearest neighbours through (phantom) elastic links with which we associate a relaxation time scale τ_E (yielding an effective elastic time scale $\tau_E N_b(N_b + 1)/6$ for the filament [27, 35]), thus rendering our elasto-inertial chains extensible (and fully flexible). The dynamics of these model filaments are then completely determined by the coupled equations of motion for the inter-bead separation

vectors $\mathbf{r}_j = \mathbf{x}_{j+1} - \mathbf{x}_j$ and the center-of-mass \mathbf{x}_c :

$$\begin{aligned} \tau_p \ddot{\mathbf{r}}_j = & [\mathbf{u}(\mathbf{x}_{j+1}, t) - \mathbf{u}(\mathbf{x}_j, t) - \dot{\mathbf{r}}_j] + A [\boldsymbol{\xi}_{j+1}(t) - \boldsymbol{\xi}_j(t)] \\ & + \frac{1}{4\tau_E} (f_{j-1}\mathbf{r}_{j-1} - 2f_j\mathbf{r}_j + f_{j+1}\mathbf{r}_{j+1}) \end{aligned} \quad (1)$$

$$\tau_p \ddot{\mathbf{x}}_c = \left(\frac{1}{N_b} \sum_{j=1}^{N_b} \mathbf{u}(\mathbf{x}_j, t) - \dot{\mathbf{x}}_c \right) + \frac{A}{N_b} \sum_{j=1}^{N_b} \boldsymbol{\xi}_j(t) - \tau_p g \hat{\mathbf{z}}. \quad (2)$$

Here, we use the FENE (finitely extensible nonlinear elastic) interaction $f_j = (1 - |\mathbf{r}_j^2|/r_m^2)^{-1}$, with a prescribed maximum inter-bead length r_m , to model the springs. Independent white noises $\boldsymbol{\xi}_j(t)$, with a coefficient $A^2 = \frac{r_0^2}{6\tau_E}$, are imposed on the beads to set the equilibrium length r_0 for each segment of our filament (in the absence of flow). We choose a coordinate system such that the acceleration due to gravity g acts along the negative z -axis; the resulting gravitational forces acting on the beads cancel out from Eq. (1) but still have an implicit effect on the dynamics of segments, via their action on the motion of the center-of-mass (which in turn determines the velocities sampled by the beads). Finally, the time-scales τ_p and τ_E , as well as the acceleration due to gravity g , allow us to define non-dimensional numbers in terms of analogous (small-scale) quantities of the carrier turbulent flow, namely the Kolomogorov time $\tau_\eta \equiv \sqrt{\nu/\epsilon}$ and acceleration $a_\eta \equiv (\epsilon^3/\nu)^{1/4}$, where ϵ is the mean energy dissipation rate of the flow. The dynamics of our filaments are thus completely determined by the Stokes number $St \equiv \tau_p/\tau_\eta$ (a measure of the inertia), the Froude number $Fr \equiv a_\eta/g$ (a measure of the force of gravity), and the Weissenberg number $Wi \equiv \frac{N_b(N_b+1)\tau_E}{6\tau_\eta}$ (a measure of elasticity).

Note that this simple model disregards inter-bead, hydrodynamic and excluded volume interactions, as well as bending stiffness [29], in an effort to more clearly reveal the fundamental interplay between elasticity, inertia, and gravitational and turbulent acceleration. It is important to point out that other models of filament dynamics, particularly in the context of turbulent transport, are available [30–33]. However, studies for low Reynolds number flow show [20] that the bead-spring approach to filaments still remains an important framework [36–39] because of the limitations of models based on slender-body theory [40, 41].

In our direct numerical simulations, we solve Eqs (1)–(2), using a second-order Runge-Kutta scheme, together and simultaneously with the three-dimensional, incompressible Navier-Stokes equations, driven to a statistically stationary state by using a constant energy injection scheme. To simulate the carrier flow, we use a de-aliased pseudo-spectral algorithm, spatially discretize the Navier-Stokes equations on a 2π periodic cubic box with

$N^3 = 512^3$ collocation points, and use a second-order slaved Adams-Bashforth scheme for time integration [42]. The fluid velocity $\mathbf{u}(\mathbf{x}, \mathbf{t})$ obtained on the regular periodic grid is interpolated, using trilinear interpolation, to obtain the velocity $\mathbf{u}(\mathbf{x}_{j+1}, t)$ at the bead positions. We choose the coefficient of viscosity $\nu = 10^{-3}$ to obtain a Taylor-scale Reynolds number $Re_\lambda \approx 200$. We evolve an ensemble of 10^4 filaments, each with an equilibrium length $r_0 \approx 47\eta$ and $N_b = 10$ beads (we have checked that our results remain qualitatively unchanged if we use a fewer number of beads, $N_b = 5$), and consider various values of Wi , St and Fr .

We begin our study by examining the fluctuating settling velocities $v_z \equiv \dot{\mathbf{x}}_c \cdot \hat{\mathbf{z}}$ of the filaments. Let us first consider the mean value $\langle v_z \rangle$, where the angular brackets denote an average over the ensemble of chains and over time in the statistically stationary state. From Eq. (2), denoting $a_z \equiv \ddot{\mathbf{x}}_c \cdot \hat{\mathbf{z}}$ as the vertical acceleration in the z direction, the assumption of a mean settling velocity implies, by definition, that $\langle a_z \rangle = 0$. Furthermore, since the noises are independent and of zero-mean, we obtain $\langle v_z \rangle = \langle \bar{u}_z \rangle - \tau_p g$, where $\tau_p g$ is the terminal settling velocity in a still-fluid, and $\bar{u}_z \equiv \frac{1}{N_b} \sum_{j=1}^{N_b} u_z(\mathbf{x}_j, t)$ is the average z -component of the fluid velocity field sampled by the filament. If an object uniformly samples the flow, as tracer particles do, then $\langle \bar{u}_z \rangle = 0$. However, this is typically not the case for non-tracers: Heavy inertial particles (with $St > 0$) are known to preferentially sample descending regions of the flow, leading to $\langle \bar{u}_z \rangle < 0$ and thus an enhanced mean settling velocity. The magnitude of this effect, which may be quantified through $\Delta_V = \langle v_z \rangle / \tau_p g - 1 = -\langle \bar{u}_z \rangle / \tau_p g$, varies non-monotonically with St as explained in [7].

Now, as instantiated by our model, a filament can be thought of as a string of elastically-linked, inertial particles. So, how does this internal linking impact the mean settling velocity of filaments? Figure 1 answers this question by presenting simulation results of Δ_V as a function of St , for filaments with $Fr = 2$ (see the inset for $Fr = 0.5$) and various values of Wi , as well as for free inertial particles (whose dynamics are given by Eq. (2) with $A = 0$ and $N_b = 1$). Clearly, the links counter-act the preferential sampling behaviour of inertial particles, resulting in a weaker enhancement of $\langle v_z \rangle$ for filaments. Indeed, at very small St and for small to moderate Wi , Δ_V becomes negative and these filaments settle slightly *slower* than they would in a still fluid. Figure 1 also suggests that the settling velocity is relatively insensitive to the elasticity of the filaments, a rather surprising observation which is reinforced below by considering the fluctuations about the mean value.

The probability distribution function (pdf) of v_z , illustrated in the inset of Fig. 2, shows that the turbulent flow can produce strong temporal fluctuations—much greater than Δ_V —which become increasingly large and non-Gaussian (the black lines are Gaussian fits) as St/Fr

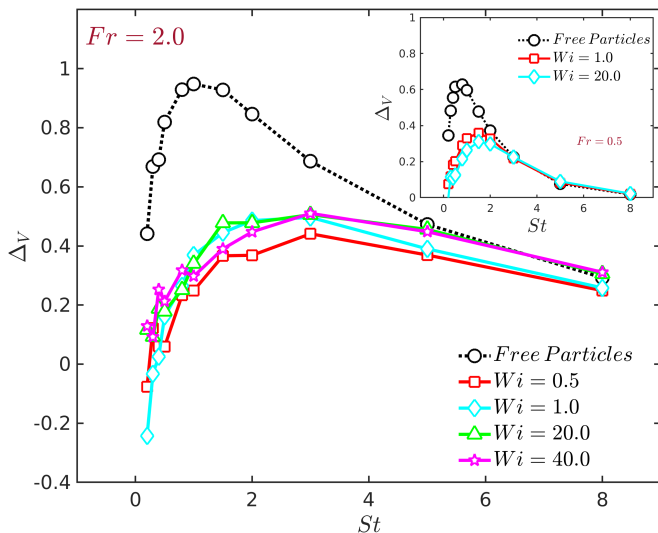


FIG. 1. Plot of the relative enhancement in the mean settling velocity Δ_V , over the still fluid value, as a function of St , for free, inertial, point particles and for filaments with different values of Wi . The inset shows results for a smaller Fr than the main panel.

increases (the relevance of this ratio becomes clear below). The magnitude of these fluctuations is best quantified through the normalised variance $\sigma \equiv \frac{\langle v_z^2 \rangle}{\langle v_z \rangle^2} - 1$ of the distribution. To obtain a theoretical estimate for this variance, we use Eq. (2) to calculate the second moment of the settling velocity $\langle v_z^2 \rangle$. Noting that $\sum_{j=1}^{N_b} \sum_{k=1}^{N_b} \langle \xi_{j,z}(t) \xi_{k,z}(t') \rangle = C \delta_{j,k} \delta(t - t')$, where the subscript z denotes the z -components of the noise and C is a constant (which absorbs the N_b factor) with the dimension of inverse time, we obtain $\langle v_z^2 \rangle = \langle \bar{u}_z^2 \rangle + \tau_p^2 g^2 + \tau_p^2 \langle a_z^2 \rangle + CA^2$, which leads to the non-dimensional, normalised variance

$$\sigma = \frac{\langle \bar{u}_z^2 \rangle + CA^2}{(a_\eta \tau_\eta)^2} \left(\frac{St}{Fr} \right)^{-2}, \quad (3)$$

where, to extract the leading order behaviour, we set $\langle a_z^2 \rangle$ to zero (the validity of this approximation is addressed later) and use $\Delta_V < 1$.

This result is further simplified by the observation, from our simulations, that $\langle \bar{u}_z^2 \rangle \approx (3/2)E$, where E is the mean kinetic energy of the flow. Furthermore, the small additive contribution of the noise to the variance, $CA^2 \propto 1/Wi$, is not relevant to understanding the effect of the turbulent flow on settling. (Indeed, one could use a non-stochastic, fixed equilibrium length, via a spring force proportional to $f_j(r_j - r_0)$, without affecting the qualitative dynamics of the chains in flow [29].) It follows, therefore, that $\sigma \sim (St/Fr)^{-2}$; the variance only depends on a single settling factor St/Fr , which is the ratio of the still-fluid terminal settling velocity $\tau_p g$ to the Kolmogorov-scale velocity of the turbulent flow $u_\eta = a_\eta \tau_\eta$.

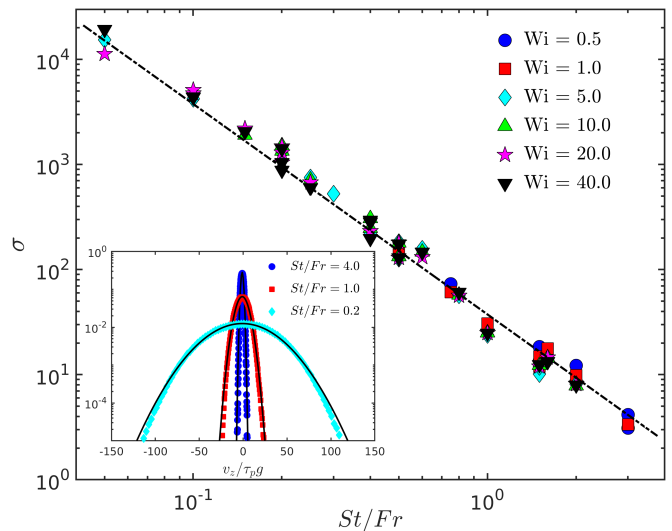


FIG. 2. Loglog plot of the normalised variance σ as a function of St/Fr ; the different symbols correspond to different values of Wi (see legend) with the thick, black dashed line showing $(St/Fr)^{-2}$. In the inset, we show representative plots of the pdfs (from which σ is extracted) of the settling speed v_z rescaled by the corresponding $\tau_p g$ for $Wi = 40$ and different values of St/Fr ; the black lines are Gaussian fits.

Motivated by this scaling result, we plot the value of σ obtained from our simulations, carried out by varying Wi , St and Fr *independently* over a range of values, against St/Fr in Fig. 2. We see that the leading order behaviour of the variance matches the scaling prediction $\sigma \sim (St/Fr)^{-2}$ (dotted line) remarkably well, over a wide range of Wi . Clearly, the extent of elasticity and therefore the stretching of the filament does not appreciably impact the settling velocity statistics.

Before proceeding, it is useful to revisit the approximation $\langle a_z^2 \rangle / g^2 \approx 0$ which lead to Eq. (3). While our simulation data does not allow us direct access to this quantity, we can estimate its value by calculating the residual obtained on substituting our data into Eq. (3). We find (not shown) that $\langle a_z^2 \rangle / g^2$ is practically independent of Wi , and although it has non-negligible values they are not large enough to disrupt the leading-order scaling with St/Fr , as is evident in Fig. 2.

So far, we have only considered the settling of the filament as a whole. However, unlike for instance spherical particles, these filaments have additional internal degrees of freedom which raise new questions, of which perhaps the most interesting is to understand how the filaments tumble as they descend through the turbulent flow. It is useful to recall that the tumbling of individual polymers—small elastic chains unaffected by inertia or gravity—has been studied in the context of simple shear flows [43, 44].

To study tumbling quantitatively, we consider the dynamics of the end-to-end vector $\mathbf{R} \equiv \sum_{j=1}^{N_b-1} \mathbf{r}_j$. In

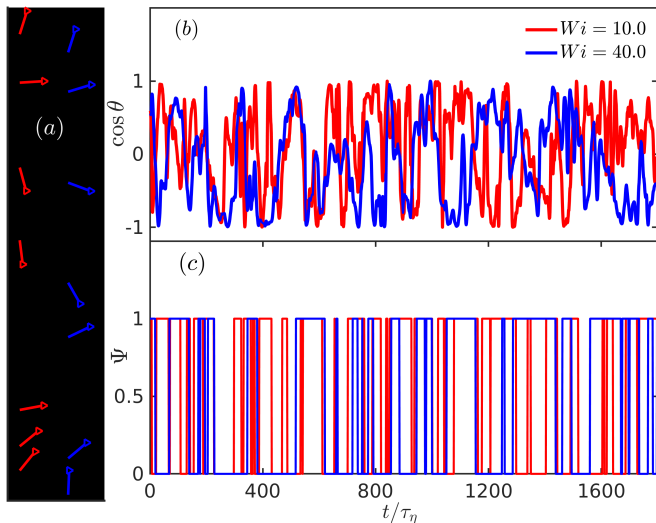


FIG. 3. (a) Representative snapshots of the end-to-end vectors \mathbf{R} of two filaments with $Wi = 10$ (red) and 40 (blue) at different times (increasing downwards) as they sediment ($St = 2$, $Fr = 0.5$); the vectors are projected on a two-dimensional plane to illustrate the change in orientation θ with respect to the direction of gravity $-\hat{\mathbf{z}}$. Plots of (b) $\cos \theta$ and (c) Ψ (see text) of the same filaments as a function of non-dimensional (with τ_η) time: $\Psi = 1(0)$ corresponds to an “up” (“down”) state of our filaments.

Fig. 3(a), we show typical time traces of the end-to-end vector projected on a two-dimensional plane, for two sedimenting filaments with different Wi (and $St = 2$, $Fr = 0.5$). Clearly the filaments undergo complicated *rotational* dynamics accompanied by tumbling events. This behaviour is quantified through the cosine of the angle made by \mathbf{R} with the z -axis, via $\mathbf{R} \cdot \hat{\mathbf{z}} = R \cos \theta$, where $R = |\mathbf{R}|$. In Fig. 3(b), we show plots of the time-series of $\cos \theta$ for the two filaments shown in panel (a). This time series illustrates the seemingly continuous changes in the orientation of the settling filaments with a suggestion that less elastic filaments tumble more frequently. Such observations naturally lead us to (a) suitably define the *state* Ψ of the filament as being either “up” or “down” and (b) to characterise the transitions between these two states.

We define the up and down states as $\Psi = 1$ for $\cos \theta \geq 0$ and $\Psi = 0$ for $\cos \theta < 0$, respectively. The apparently random switching between the two states, clearly illustrated in Fig 3(c), is quantified by calculating the pdfs $P^+(\tau)$ ($P^-(\tau)$) of the residence time τ over which the filaments remain up (down). These distributions yield the probability of a filament in an up (or down) state to continue to remain in the same state for a duration of τ . We recall that questions of this sort—the so-called persistence problems—have a special importance in areas of non-equilibrium statistical physics [45–48] and have, more recently, been adapted to understand the geometrical aspects of turbulent flows [49–51].

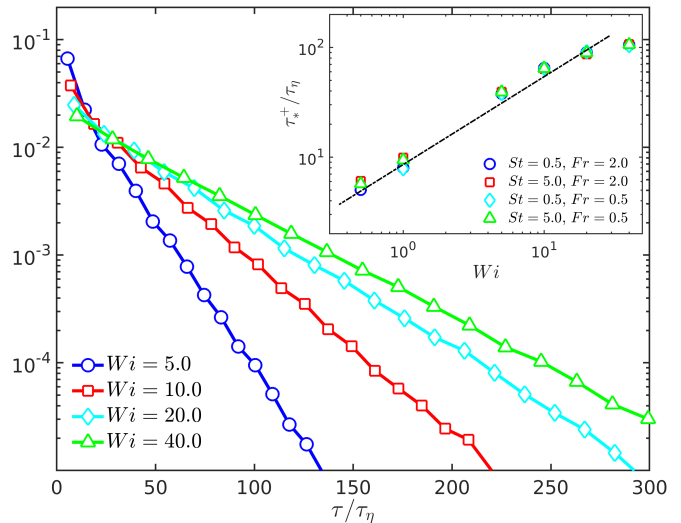


FIG. 4. Probability distribution functions $P^+(\tau)$ of the residence time in the up ($\Psi = 1$) state for filaments with $St = Fr = 1.0$ and different values of Wi . (Inset) Log-log plot of the characteristic time-scale τ_*^+ versus Wi for different values of St and Fr ; the thick black line indicates a scaling of $Wi^{4/5}$.

In Fig. 4, we show semi-log plots of $P^+(\tau)$ for filaments with $St = Fr = 1.0$, but different degrees of elasticity. [We have confirmed, by varying the range of angles θ which define an up or down state, that the precise definition of these states does not affect the results qualitatively; furthermore, $P^+(\tau) = P^-(\tau)$ and hence $\tau_*^+ = \tau_*^-$, because the problem is symmetric to the transformation $r_j \rightarrow -r_j$ which reverses the end-to-end vector.] These distributions clearly show an exponential fall-off [44]: $P^+(\tau) \sim \exp(-\tau/\tau_*^+)$, which indicates that tumbling manifests as a Poisson process. The characteristic time scale τ_*^+ has a weak dependence on St and Fr , but increases systematically (see Ref. [44] for single polymers in a shear flow) with Wi , as seen in the inset of Fig. 4.

Why do more extensible filaments require longer times to tumble? The answer lies in the connection between the dynamic length of a filament and its tumbling. We expect a highly stretched, long filament that spans multiple flow eddies to have a lower probability of experiencing the sequence of coordinated drag forces required to cause a transition in its orientation. To test this hypothesis, we calculate the average end-to-end length of a filament over each interval of time spent in the up state $\langle R \rangle_+$. When a transition occurs, we record $\langle R \rangle_+$ along with the persistence time τ , which then allows us to obtain the pdf of τ conditioned on the time-averaged length of the filament. Fig 5 shows these conditioned pdfs for relatively short (dashed line) and long (solid line) filaments, defined as those with $\langle R \rangle_+ < \ell_1$ and $\langle R \rangle_+ > \ell_2$ ($\ell_1 < \ell_2$), where the values of the thresholds depend on Wi and are given in the figure caption (small variations in these values do not affect our conclusions). Two values of Wi are con-

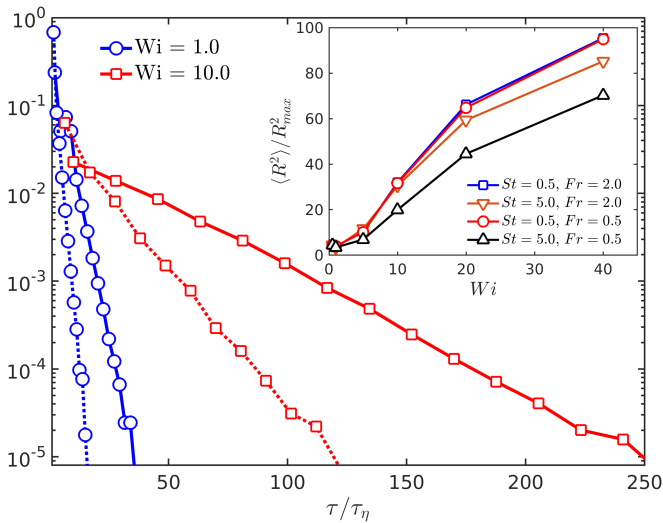


FIG. 5. Conditioned probability distribution functions of time spent in the up ($\Psi = 1$) state, for filaments with relatively small ($\langle R \rangle_+ < \ell_1$; dashed lines) and large ($\langle R \rangle_+ > \ell_2$; solid lines) time-averaged lengths. The values of the thresholds for the two cases are $\ell_1 = 9\eta$, $\ell_2 = 20\eta$ for $Wi = 1$, and $\ell_1 = 40\eta$, $\ell_2 = 65\eta$ for $Wi = 10$. In both cases, $St = Fr = 1.0$. (Inset) Plot of normalised $\langle R^2 \rangle$, versus Wi for different values of St and Fr .

sidered, and in both cases we see that when filaments are more stretched they do indeed take a longer time to tumble. (Note that a similar inverse relationship between length and tumbling rate has been recently observed in experiments on rigid, neutrally buoyant fibres in isotropic turbulence [34].) Now, as Wi increases, the filaments become more extensible and the distribution of R broadens. This is demonstrated by the inset of Fig 5, which presents the variation of $\langle R^2 \rangle$ with Wi , for all chains in the ensemble over all time. As a result, a larger Wi filament is much more likely to be in a highly stretched state, which explains its tendency to persist in a given orientation for a longer time before tumbling. The consequent increase of τ_+ with Wi , shown in the inset of Fig. 4, appears to follow a power-law (the fitted dashed-line has an exponent of $4/5$) for small to moderate Wi , but then begins to level-off at large Wi , as the filament approaches its maximum length.

To summarise, we have analyzed two complementary aspects of the dynamics of long and heavy, elastic filaments in a turbulent flow: the fluctuating settling velocity, and the transitions in vertical orientation associated with tumbling. For a given turbulent flow, we have found, rather surprisingly, that to leading order the weight of the filament only impacts its settling velocity (via the St dependence of Δ_V and the $(St/Fr)^{-2}$ scaling of σ) while the elasticity and consequent stretching of the filament only affects its tumbling.

The Poisson distribution of tumbling times, uncovered by our persistence analysis, brings to mind the Poisso-

nian *back-and-forth* motion of filamentary, motile microorganisms. This tumbling-like motion is thought to be an efficient strategy for foraging [52, 53], but given that the Reynolds number of oceanic turbulence [54] is similar to that in our study, it is tempting to consider in future works whether the tumbling of marine filamentary microorganisms are a consequence of active strategy or physical inevitability. Admittedly, these microorganisms are motile and much smaller than our filaments; nevertheless, our results should motivate work on longer marine organisms and their journey as they settle in the ocean. Furthermore, this study is relevant to the sedimentation of passive marine pollutants, such as plastic debris from fishing gear [24, 25], as well as to fibre suspensions in industry [21].

We are grateful to Dario Vincenzi for many insightful discussions and for introducing us to this problem. RKS and SSR also thank A. Kundu for useful discussions. The simulations were performed on the ICTS clusters *Contra* and *Tetris* as well as the work stations from the project ECR/2015/000361: *Goopy* and *Bagha*. SSR and RKS acknowledge the support of the DAE, Govt. of India, under project no. 12-R&D-TFR-5.10-1100 and SSR is grateful to the DST (India) project MTR/2019/001553 for financial help. JRP is thankful for support from the IIT-Bombay IRCC Seed Grant.

* rahul.singh@icts.res.in

- [1] M. Maxey, *J. Fluid Mech.* **174**, 441 (1987).
- [2] L.-P. Wang and M. Maxey, *J. Fluid Mech.* **256**, 27 (1993).
- [3] A. Aliseda, A. Cartellier, F. Hainaux, and J. C. Lasheras, *J. Fluid Mech.* **468**, 77–105 (2002).
- [4] S. Ghosh, J. Dávila, J. Hunt, A. Srdic, H. Fernando, and P. Jonas, *Proceedings of the Royal Society A: Mathematical, Physical and Engineering Sciences* **461**, 3059 (2005).
- [5] O. Ayala, B. Rosa, L.-P. Wang, and W. Grabowski, *New J. Phys.* **10**, 075015 (2008).
- [6] J. Davila and J. Hunt, *J. Fluid Mech.* **440**, 117 (2001).
- [7] J. Bec, H. Homann, and S. S. Ray, *Phys. Rev. Lett.* **112**, 184501 (2014).
- [8] K. Gustavsson, J. Jucha, A. Naso, E. Lévêque, A. Pumir, and B. Mehlig, *Phys. Rev. Lett.* **119**, 254501 (2017).
- [9] P. Anand, S. S. Ray, and G. Subramanian, *Phys. Rev. Lett.* **125**, 034501 (2020).
- [10] P. A. Vaillancourt and M. K. Yau, *Bulletin of the American Meteorological Society* **81**, 285 (2000).
- [11] G. Falkovich, A. Fouxon, and M. G. Stepanov, *Nature* **419**, 151 (2002).
- [12] R. A. Shaw, *Annual Review of Fluid Mechanics* **35**, 183 (2003).
- [13] E. Bodenschatz, S. P. Malinowski, R. A. Shaw, and F. Stratmann, *Science* **327**, 970 (2010).
- [14] R. Monchaux, M. Bourgoin, and A. Cartellier, *Int. J. Multiph. Flow* **40**, 1 (2012).
- [15] A. J. Baran and P. N. Francis, *Quarterly Journal of the Royal Meteorological Society* **130**, 763 (2004).

- [16] M. W. Gallagher, P. J. Connolly, J. Whiteway, D. Figueras-Nieto, M. Flynn, T. W. Choularton, K. N. Bower, C. Cook, R. Busen, and J. Hacker, *Quarterly Journal of the Royal Meteorological Society* **131**, 1143 (2005).
- [17] A. K. Pandit, H. S. Gadhavi, M. Venkat Ratnam, K. Raghunath, S. V. B. Rao, and A. Jayaraman, *Atmospheric Chemistry and Physics* **15**, 13833 (2015).
- [18] G. A. Voth and A. Soldati, *Annual Review of Fluid Mechanics* **49**, 249 (2017).
- [19] S. Alben, M. Shelley, and J. Zhang, *Nature* **420**, 479 (2002).
- [20] B. Marchetti, V. Raspa, A. Lindner, O. du Roure, L. Bergougnoux, E. Guazzelli, and C. Duprat, *Phys. Rev. Fluids* **3**, 104102 (2018).
- [21] F. Lundell, L. D. Soderberg, and P. H. Alfredsson, *Annu. Rev. Fluid Mech* **43**, 195 (2011).
- [22] D. K. A. Barnes, F. Galgani, R. C. Thompson, and M. Barlaz, *Philosophical Transactions of the Royal Society B: Biological Sciences* **364**, 1985 (2009).
- [23] A. Lusher, “Microplastics in the marine environment: Distribution, interactions and effects,” in *Marine Anthropogenic Litter*, edited by M. Bergmann, L. Gutow, and M. Klages (Springer International Publishing, Cham, 2015) pp. 245–307.
- [24] M. Stelfox, J. Hudgins, and M. Sweet, *Marine Pollution Bulletin* **111**, 6 (2016).
- [25] L. Lebreton, B. Slat, F. Ferrari, B. Sainte-Rose, J. Aitken, R. Marthouse, S. Hajbane, S. Cunsolo, A. Schwarz, A. Levivier, K. Noble, P. Debeljak, H. Maral, R. Schoeneich-Argent, R. Brambini, and J. Reisser, *Sci. Rep.* **8**, 4666 (2018).
- [26] R. B. Bird, C. F. Curtiss, R. C. Armstrong, and O. Hassager, *Dynamics of Polymeric Liquids* (John Wiley and Sons, New York, 1977).
- [27] J. R. Picardo, D. Vincenzi, N. Pal, and S. S. Ray, *Phys. Rev. Lett.* **121**, 244501 (2018).
- [28] R. Singh, M. Gupta, J. R. Picardo, D. Vincenzi, and S. S. Ray, *Phys. Rev. E* **101**, 053105 (2020).
- [29] J. R. Picardo, R. Singh, S. S. Ray, and D. Vincenzi, *Phil. Trans. R. Soc. A* **378**, 20190405 (2020).
- [30] C. Brouzet, G. Verhille, and P. Le Gal, *Phys. Rev. Lett.* **112**, 074501 (2014).
- [31] G. Verhille and A. Bartoli, *Exp. Fluids* **57**, 117 (2016).
- [32] M. E. Rosti, A. A. Banaei, L. Brandt, and A. Mazzino, *Phys. Rev. Lett.* **121**, 044501 (2018).
- [33] S. Allende, C. Henry, and J. Bec, *Phys. Rev. Lett.* **121**, 154501 (2018).
- [34] T. B. Oehmke, A. D. Bordoloi, E. Variano, and G. Verhille, ArXiv e-prints (2020), arXiv:2011.08546.
- [35] S. Jin and L. R. Collins, *New J. Phys.* **9**, 360 (2007).
- [36] M. Cosentino Lagomarsino, I. Pagonabarraga, and C. P. Lowe, *Phys. Rev. Lett.* **94**, 148104 (2005).
- [37] X. Schlagberger and R. R. Netz, *Europhysics Letters (EPL)* **70**, 129 (2005).
- [38] I. Llopis, I. Pagonabarraga, M. Cosentino Lagomarsino, and C. P. Lowe, *Phys. Rev. E* **76**, 061901 (2007).
- [39] B. Delmotte, E. Climent, and F. Plouraboué, *Journal of Computational Physics* **286**, 14 (2015).
- [40] R. G. Cox, *J. Fluid Mech.* **44**, 791–810 (1970).
- [41] X. Xu and A. Nadim, *Physics of Fluids* **6**, 2889 (1994).
- [42] M. James and S. S. Ray, *Sci. Rep.* **7**, 12231 (2017).
- [43] S. Geraschenko and V. Steinberg, *Phys. Rev. Lett.* **96**, 038304 (2006).
- [44] A. Celani, A. Puliafito, and K. Turitsyn, *Europhysics Letters (EPL)* **70**, 464 (2005).
- [45] S. N. Majumdar, C. Sire, A. J. Bray, and S. J. Cornell, *Phys. Rev. Lett.* **77**, 2867 (1996).
- [46] B. Derrida, V. Hakim, and R. Zeitak, *Phys. Rev. Lett.* **77**, 2871 (1996).
- [47] S. N. Majumdar, *Current Science* **77**, 370 (1999).
- [48] A. J. Bray, S. N. Majumdar, and G. Schehr, *Advances in Physics* **62**, 225 (2013).
- [49] P. Perlekar, S. S. Ray, D. Mitra, and R. Pandit, *Phys. Rev. Lett.* **106**, 054501 (2011).
- [50] B. Kadoch, D. del Castillo-Negrete, W. J. T. Bos, and K. Schneider, *Phys. Rev. E* **83**, 036314 (2011).
- [51] A. Bhatnagar, A. Gupta, D. Mitra, R. Pandit, and P. Perlekar, *Phys. Rev. E* **94**, 053119 (2016).
- [52] R. H. Luchsinger, B. Bergersen, and J. G. Mitchell, *Biophysical Journal* **77**, 2377 (1999).
- [53] R. Stocker, *Proceedings of the National Academy of Sciences* **108**, 2635 (2011).
- [54] J. Jimenez, *Scientia Marina* **61**, 47 (1997).